Progress In Electromagnetics Research M, Vol. 22, 91–107, 2012

DOUBLE DIRECTIONAL CHANNEL MEASUREMENTS IN AN ARCHED TUNNEL AND INTERPRETATION USING RAY TRACING IN A RECTANGULAR TUNNEL

C. Garcia-Pardo[1, *], J.-M. Molina-Garcia-Pardo[1], M. Lienard[2], D. P. Gaillot[2], and P. Degauque[2]

[1]Information Technologies and Communications Department, Technical University of Cartagena, 30202, Spain

[2]IEMN/TELICE Laboratory, University of Lille, 59655 Villeneuve D'Ascq, France

Abstract—The objective of this paper is to study the wideband characteristics of the radio channel in a tunnel environment, not only the delay spread, but also the angle of departure/arrival of the rays, their relative weights and their delays, which are important values for Multiple-Input Multiple-Output applications. In order to achieve this goal, a measurement campaign has been carried out in a straight arched tunnel over a frequency band extending from 2.8 to 5.0 GHz and distance varying from 50 m up to 500 m. First, the variations of the channel impulse response and of the delay spread versus the distance between the transmitter and the receiver are analyzed. Then, the bidirectional channel characteristics have been extracted from the measured channel matrices using a high resolution estimation algorithm. The main contribution of this paper is to clearly show the quantitative variation of the delay spread and the angle of departure/arrival of the rays along a real tunnel and to investigate the possibility of using the ray theory in a rectangular tunnel to interpret experimental results obtained in an arched tunnel.

Received 1 July 2011, Accepted 5 October 2011, Scheduled 2 December 2011

* Corresponding author: Concepcion Garcia-Pardo (conchi.gpardo@upct.es).

1. INTRODUCTION

Experimental works on propagation characteristics in tunnels have covered scenarios ranging from mine galleries and old underground quarries, to road and railway tunnels. Underground mine tunnels are characterized by very rough surfaces and in most cases there is no line of sight between the transmitter (Tx) and the receiver (Rx). Measurements at 900 MHz in typical coal mine operational zones for vertical and horizontal polarization are reported in [1]. Results of wideband measurements and statistical modeling in the range of 150–900 MHz are given in [2] and at 2.4 GHz and 5.8 GHz in [3]. Channel modeling and an analysis of wireless networks at 500 MHz or 1 GHz are described in [4].

The geometrical structure of a road or railway tunnel is far simpler than that of a mine tunnel. The walls of arc-shaped tunnels are usually quite smooth and they are often straight over a long distance. One can thus expect to have quite different channel characteristics compared to those of a mine. In [5], narrow band measurements at 2 GHz in a railway tunnel are described and the path loss, the probability distribution with respect to fading widths and the distance between successive fading are given. The results of narrowband and wideband propagation measurements conducted at 900 and 1800 MHz in five tunnels are presented in [6]. Narrowband propagation is characterized in terms of power distance law, slow fading, and fast fading statistics, whereas the rms delay spread is the chosen metric. Thus, it is interesting to extend the previous experimental approaches in order to obtain quantitative results about the bidirectional channel characteristics, such as the angle of departure (AoD) and the angle of arrival (AoA) of the paths and the angular spread along the tunnel. Furthermore, in case of a high speed transmitting/receiving mobile, the knowledge of the AoA/AoD can be used when defining a tapped delay line model for the channel, since the Doppler effect can be introduced on each ray, i.e., on each tap.

The main application of our work deals with automatic underground subways, since a large amount of data must be exchanged either between two trains following one another or between a train and the track. In this case, the tunnel can be considered as empty, the influence of a train moving on an adjacent track being out of the scope of this paper. The frequency band of analysis extends from 2.8 to 5 GHz and the distance between the transmitter (Tx) and the receiver (Rx) varies from 50 m up to 500 m. Multiple-Input Multiple-Output (MIMO) transmission techniques have been proposed [7–9] to improve the performances of the link, but the result is strongly dependent on

the channel properties. A measurement campaign was thus needed since, to our knowledge, delay spread and double directional channel characteristics have never been measured continuously in ranges up to 500 m in a subway environment. Unfortunately, organizing experiments in a subway tunnel is quite complicated due to the numerous operational constraints. We have thus preferred to perform our measurements in an empty straight road tunnel whose arc-shape cross-section is quite similar to the shape often encountered in subway tunnels.

Predicting and interpreting the channel characteristics inside such tunnels from a theoretical propagation model are also important in the deployment of wireless communication systems. From a mathematical point of view, the internal surface of an arched tunnel cannot be easily described using a canonical coordinate system and, consequently, no exact analytical formulation is currently available. A numerical ray-optical wave propagation model based on ray-density normalization [10], on solving vectorial parabolic equations [11] or on a ray-tube tracing method [12] have been suggested for arbitrary shaped tunnels. A formulation of the Iterative Physical Optics was developed by Aurojo et al. [13] to study the propagation in such environment, whereas a cascade impedance method is explained in [14]. Mahmoud [15] has recently presented a perturbation analysis for evaluating the propagation character of the dominant modes in uniform tunnels with cross sections that deviate from the circular shape and has also proposed a cost-effective FDTD method [16] which could be used for modeling tunnels with realistic construction profiles.

These approaches are, however, not easy to implement or not able to predict all channel characteristics. Another possibility is to drastically simplify the tunnel shape, assuming its cross section to be either rectangular or circular (canonical shape). For example, Emslie et al. [17] and Mahmoud and Wait [18], among many others, have proposed solutions for rectangular tunnels. Holloway et al. [19], Dudley and Mahmoud [20], and Mahmoud [21] have described a modal analysis of radio wave propagation in circular waveguides or in straight and curved rectangular tunnels. For easily interpreting MIMO performances, it has been previously shown that narrow band channel characteristics in an arched tunnel can be predicted with sufficient accuracy by using an equivalent rectangular tunnel [22]. It is thus interesting to know if such an approach can also be applied to the wide band analysis.

The paper is organized as follows: Section 2 gives a brief description of the experiments, including the geometry of the tunnel and the measurement system. The power delay profile and the

variation of the delay spread versus distance are examined in Section 3. The experimental values are compared to theoretical results, assuming that the tunnel has a rectangular cross section. Lastly, Section 4 presents the distribution of the AoA/AoD of the paths and their relative weights. Section 5 provides a summary and the conclusions of the work here presented.

2. DESCRIPTION OF THE EXPERIMENTAL APPROACH

The straight tunnel wherein our measurements were performed is shown in Fig. 1. This 3 km-long tunnel was closed to traffic during the experiments and the propagation channel is therefore stationary. The transverse section of the tunnel was semicircular and the diameter of the cylindrical part was 8.6 m. The maximum height was 6.1 m at the center of the tunnel. The roughness of the walls is quite low, in the order of less than 2 cm.

2.1. Measurement Equipment

The complex channel transfer function between the transmitting (Tx) and receiving (Rx) antennas has thus been obtained by measuring the S_{21} parameter with a vector network analyzer (VNA Agilent E5071B). Using a coaxial cable to connect the Tx antenna to one port of the VNA would lead to prohibitive attenuation, the maximum distance between Tx and Rx being 500 m. The signal of the Tx port of the VNA is thus connected to a distributed feedback laser transmitter (ORTEL 3541A) working in a frequency range extending from 100 MHz to 10 GHz, the amplitude flatness in this whole band being ± 2.5 dB. The optical signal is sent through a monomode fibre optics presenting a very low attenuation (2 dB/km). It is then converted back to radio

Figure 1. Straight road tunnel in which experiments were conducted.

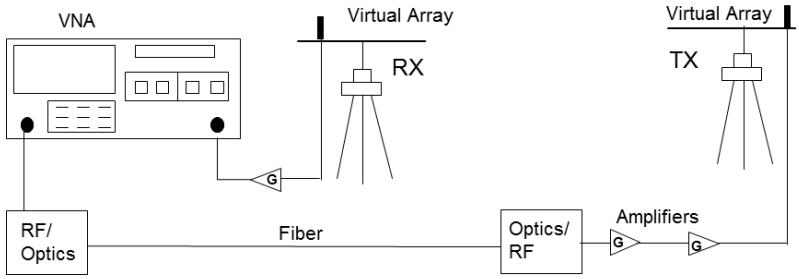

Figure 2. Principle of the channel sounder set-up [7].

frequency owing to a wideband photodiode receiver (Agere 4518B), whose amplitude flatness is the same as for the transmitter. In our frequency band of interest (2.8–5 GHz), the total loss of the optical chain is 26 dB $\pm$ 0.5 dB. The signal is thus amplified so that the output RF signal reaches a transmitter power of 20 dBm.

The Rx antenna is directly connected to the other port of the VNA using a low attenuation coaxial cable, 4 m long, a 30 dB low-noise amplifier (Nextec NBL00416) having a noise figure of 2.5 dB.

The phase stability of the fibre optics link has been checked and the calibration of the VNA takes amplifiers, cables and optic coupler into account. The block diagram of the channel sounder is depicted in Fig. 2.

The wideband biconical antennas (Electrometrics EM-6116) used in this experiment have nearly a flat gain, between 2 and 10 GHz. Indeed, the frequency response of the two antennas has been measured in an anechoic chamber, and the variation of the antenna gain was found to be less than 2 dB in our frequency range. The radiation pattern of wideband antennas is thus also slightly frequency dependent. This is not a critical point in our case since, in a tunnel, only waves impinging the tunnel walls with a grazing angle of incidence contribute to the total received power significantly. This means that, whatever the frequency, the angular spread of the received rays remains much smaller than the 3 dB beamwidth of the main antenna lobe in the E plane, equal to about 80°, the antenna being nearly omnidirectional in the H plane.

Virtual arrays were obtained by moving the Tx and Rx antennas along a rail. The position mechanical systems are remote controlled, with a precision of $\pm$0.5 mm, optic fibres connecting the step by step motors to the control unit situated near the VNA. The battery-driven mobile equipment was mounted on a wooden rolling table which was manually pulled.

2.2. Methodology

The channel frequency response has been measured for 1601 frequency points, equally spaced between 2.8 and 5 GHz, leading to a frequency step of 1.37 MHz.

The rails supporting the Tx and Rx antennas were put at a height of 1 m and centred on the same lane of this 2-lane tunnel, thus at 1/4 of the tunnel width. For each successive axial distance d, both the Tx and Rx antennas were moved in the transverse plane on a distance of 33 cm, with a spatial step of 3 cm, corresponding to half a wavelength at 5 GHz. A $(12, 12)$ transfer matrix is thus obtained, the configuration of the measurements being schematically described in Fig. 3. Fine spatial sampling was chosen for measurements in the transverse plane to be able to extract information of the direction of departure/arrival of the rays.

Due to the limited time available for such an experiment and to operational constraints, it was not possible to extensively repeat such measurements for very small steps along the tunnel axis. In the experiments described in this paper, the axial step was chosen equal to 4 m when $50\,\text{m} < d < 202\,\text{m}$ and to 6 m when $202\,\text{m} < d < 500\,\text{m}$. In such kind of experiments, an optical pulse generator is coupled to a wheel of the mobile system, the accuracy on the location of the mobile being on the order or less than 1 cm [23]. Let us mention that if the measurement system is on-board a vehicle moving in a tunnel, the time interval between two successive sampling would have to be greater than the whole time response of the measurement set up, as explained in [22].

Measurements are made in successive static conditions. At each Tx and Rx position, 5 successive recordings of field variation versus frequency are stored and averaged. A summary of the measurement parameters and equipment characteristics is summarized in Table 1.

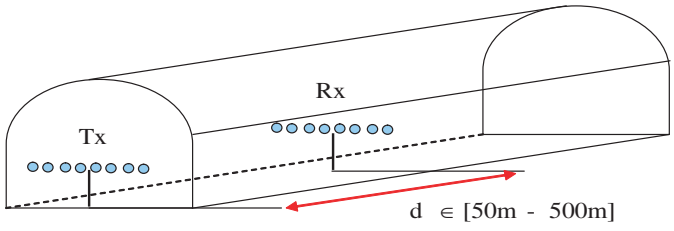

Figure 3. Configuration of the wideband measurements.

Table 1. Equipment characteristics and measurement parameters.

Frequency Band	2.8 GHz–5 GHz
Number of frequency points	1601
Antenna	Biconical antenna (Electrometrics EM-6116)
Transmitter Power	20 dBm
Dynamic Range	> 100 dB
Position in the transverse plane	12 positions every 3 cm ($\lambda/2$ at 5 GHz)
Positions along the longitudinal axis	From 50 m to 202 m every 4 m From 202 m to 500 m every 6 m
Number of acquisitions at each position	5

3. POWER DELAY PROFILE AND DELAY SPREAD

As the channel is stationary, the channel transfer function in the frequency domain $H(d, i, j, f)$ is measured with the experimental set up described in the previous paragraph. The variables i and j, varying from 1 to 12, correspond to the various locations of the antennas in the transverse plane. It must be clearly emphasized that stationary means in this case that, for each distance d, the channel is no time dependent since there is no moving object in the tunnel. However, when Rx is moving, i.e., when d varies, the channel transfer function is changing.

The complex channel impulse response at a distance d between Tx and Rx, expressed as $h(d, i, j, \tau)$, where τ represents the channel multipath delay, is then obtained by applying a Hamming window and an inverse Fourier transform to $H(d, i, j, f)$.

3.1. Power Delay Profile

For small-scale channel modeling, the average power delay profile, often simply called PDP, is found by taking the spatial average of $|h(d, i, j, \tau)|^2$ [24]. In the following examples, the axial distance d is larger than 50 m, whereas in the transverse plane, the antennas move along a maximum distance of 33 cm. Thus, for a given value of d, the propagation delay due to the difference in distances between the successive transverse locations of Tx and Rx is smaller than 0.03 ns which is quite negligible. Consequently, the PDP (d, τ) is obtained by simply averaging $|h(d, i, j, \tau)|^2$ over the 12×12 positions (i, j) of the antennas. At each distance d, the power of the strongest path of the PDP is then normalized to 0 dB. All successive normalized PDPs at

different distances have been gathered in Fig. 4.

It must be emphasized that the delays presented are always measured relative to free space delay, corresponding to the direct path. Only paths whose weights are attenuated less than 20 dB are represented in Fig. 4 and in the following figures.

It is interesting to compare these experimental results with theoretical values. However, the simulation of the propagation in an arched tunnel over a large distance and over a wide frequency band is not an easy task and, as mentioned in the introduction, we have thus chosen a very simple model based on the image theory. Indeed, we have shown in [22] that for frequencies of 500 MHz and 900 MHz it was possible to interpret both path loss and fading in this arched tunnel by means of an equivalent straight rectangular tunnel, 8 m wide and 5.6 m high, with walls of an equivalent conductivity and permittivity equal to 10^{-2} S/m and 5, respectively. Using these values, and with the same

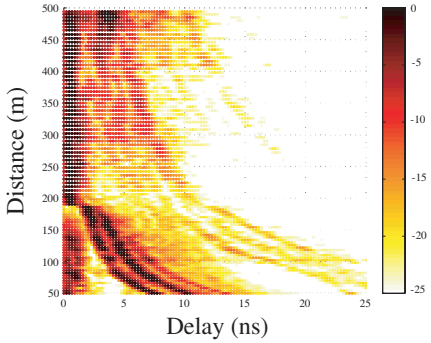

Figure 4. PDPs deduced from measurements and normalized to 0 dB corresponding to their maximum power. The color scale gives the relative power in dB. The modification in the appearance of the Figure occurring for a distance of 200 m is due to the change of the measurement step, thus of the sampling (4 m if $d < 206$ m and 6 m if $d > 206$ m). The delays between successive rays continuously decrease with distance, at least for distances smaller than 200 m.

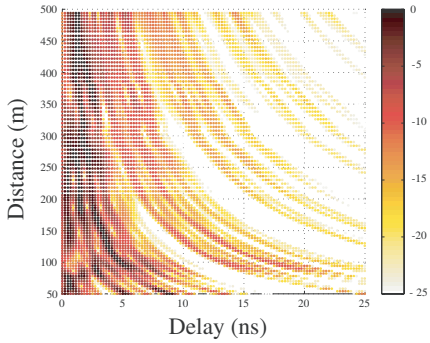

Figure 5. PDPs obtained from a theoretical propagation model, assuming a tunnel of rectangular cross section (8 m × 5.6 m) and the same frequency bandwidth as in the measurements. Only rays reflecting on the walls with a grazing angle of incidence mainly contribute to the total field. This gives rise to these typical shapes of the PDPs.

bandwidth as in the experiments (2.8–5 GHz), the PDPs deduced from the propagation model are given in Fig. 5.

At a short distance from Tx, between 50 m and 100 m, the successive paths can be clearly distinguished in both figures. At 50 m, the maximum delay, considering a relative attenuation of 10 dB referred to the strongest path, is 10–15 ns. When this distance increases, only rays impinging the tunnel wall with a grazing angle of incidence play a leading part, and this gives rise to the typical shape of the plots drawn in Figs. 4 and 5.

In these Figures, local decreases of the received power also appear. As an example, Fig. 5 shows that the signals arriving during the first 3 ns are attenuated in a zone situated at about 100 m from Tx. Indeed, even with a 2.2 GHz bandwidth, the time resolution is not high enough to separate the contribution of individual rays and destructive (or constructive) interference may occur. The ray tracing model, assuming an infinite bandwidth and a rectangular tunnel, shows that 32 rays, having a relative attenuation of less than 10 dB, arrive during a time window of 10 ns, and 10 rays reach the Rx during the first 3 ns.

3.2. Delay Spread

To obtain quantitative characteristics of the channel impulse response, a local rms delay spread D_s, associated to a single link between a Tx antenna i and a Rx antenna j is introduced. It is defined [24] as the normalized second-order central moment of $P_r(d,i,j,\tau_k) = |h(d,i,j,\tau_k)|^2$:

$$D_s(d,i,j) = \sqrt{\frac{\sum\limits_k P_r(d,i,j,\tau_k)\,\tau_k^2}{\sum\limits_k P_r(d,i,j,\tau_k)} - \left(\frac{\sum\limits_k P_r(d,i,j,\tau_k)\,\tau_k}{\sum\limits_k P_r(d,i,j,\tau_k)}\right)^2}, \quad (1)$$

where τ_k is the propagation delay.

For each transverse position of the antennas, i and j varying from 1 to 12, 144 values of D_s are obtained. Since it is interesting to point out the variation of D_s both on a small scale and on a large scale, the tunnel was divided into 4 zones. The first one extends from 50 m to 100 m and henceforth will be called the "near" zone. Other zones correspond to distance intervals from 100 m to 200 m, from 200 m to 300 m, from 300 m to 400 m and finally from 400 m to 500 m. Fig. 6 shows the complementary cumulative distribution function (CCDF) of the local D_s, deduced from experimental data.

If we consider a probability of 0.5, the curves in Fig. 6 show that the D_s is in the order of 3.6 ns in the near zone (50 m–100 m), but then

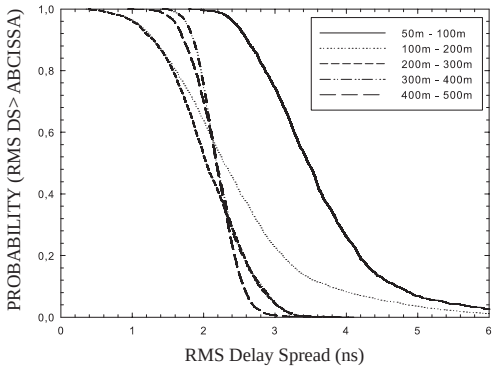

Figure 6. CCDFs of the local rms delay spread deduced from experimental data. The RMS delay spread decreases rapidly when the distance increases up to 200 m, but then remains on the order of 2 to 3 ns at larger distance.

decreases to 2.5 ns beyond 100 m and does not vary very much with distance. This can also be observed by visually interpreting Fig. 5. For a rectangular tunnel, 8 m × 5.6 m, the theoretical values of the D_s deduced from the ray approach are larger and vary from 6 ns in the near zone to 4 ns beyond 100 m. The difference may be due to the idealized rectangular shape of the tunnel in the theoretical model, instead of the curved shape of the tunnel where experiments took place. The values of D_s can be compared to those measured in an empty tunnel, without obstacles, and described by other authors as in [3] and [6]. In a 70 m long mine gallery, it was shown [3] that D_s in the 2.4 GHz band is less than or equal to 6.3 ns for 50% of all locations. The corresponding value for the 5.8 GHz band is 5 ns. Delay spread in a rectangular concrete subway tunnel, 3.5 m wide and 2.6 m high, at a carrier frequency of 1.8 GHz and over a 400 MHz band was found to be equal to 5.5 ns for a 50 m separation between the transmit and receive antennas [6].

In Fig. 6, we can also note that when the distance increases from 100 m to 500 m, the slopes of the CCDF curves become steeper corresponding to a decrease of the spread of the D_s. For example, if we consider a probability interval of 0.1–0.9, D_s is between 1.3 and 3.9 ns within the 100 m–200 m range from Tx and between 1.9 and 2.5 ns within the 400 m–500 m range from Tx.

The characteristics of the different paths, such as their amplitude, delay, and their AoA/AoD, can be extracted from our measurements by applying the RiMAX high resolution algorithm, the description of parameter extraction process being described in [25, 26]. This algorithm is a recently developed multidimensional maximum-

likelihood high-resolution channel parameters estimator. It is based on the assumption that the radio channel can be modeled as a superposition of a number of finite specular-alike propagation paths and dense multipath components. The algorithm iteratively seeks propagation paths and optimizes their characteristics. It does not require a prior knowledge of the number of dominant propagation paths.

4. BIDIRECTIONAL CHANNEL CHARACTERISTICS

The virtual antenna arrays were situated on the horizontal plane, the array axis being perpendicular to the tunnel axis. It is thus only possible to compute the azimuth φ of arrival or departure of the rays in this plane and defined as the horizontal angular distance from the tunnel axis z to the direction of the rays. A 1D array is not able to distinguish rays propagating along positive or negative values of z, i.e., from or towards the transmitter. However, this is not critical for our application since in an empty tunnel, no reflection giving rise to a backward propagation may occur.

In a preliminary step, the theoretical azimuth power spectrum $APS\ (d, \varphi)$ [27] versus the distance between Tx and Rx, has been directly calculated from the locations of the images of Tx in the ray tracing model, assuming a rectangular tunnel $8\,\mathrm{m} \times 5.6\,\mathrm{m}$ as mentioned in Section 3.1.

For each axial distance, the power of the strongest ray, corresponding to the direct path, is normalized to 0 dB. In such a rectangular tunnel, many rays arrive with the same azimuth φ and thus only the APS of the most powerful rays are presented in Fig. 7. Their relative weights in the successive transverse planes (between 50 m and 500 m) are expressed in dB and are given by the color scale on the right hand side of the figure.

There is no axial symmetry since the Tx and Rx antennas are situated at a transverse distance of 1/4 of the tunnel width, as in the case in the experiments. Fig. 7 clearly shows a decrease in the angle of arrival (AoA) with distance. For example, if we consider the rays having a relative attenuation equal to or smaller than 20 dB, the AoAs are between $+/-30^\circ$ if $d = 50\,\mathrm{m}$ but decreases to $+/-\ 10^\circ$ when $d = 400\,\mathrm{m}$.

In order to optimize all the parameters of the narrow band high resolution algorithm, one can also deduce $APS\ (d, \varphi)$ from the theoretical channel transfer functions $H\ (d,\ i,\ j,\ f)$ at each distance d for the 12×12 possible links. By conducting a parametric study, it appears that the best results, shown in Fig. 8, were obtained with 146

frequency points, in a 200 MHz band (between 4.8 and 5 GHz). One can mention that the results on the APS of the angle of departure (AoD) are quite similar to those of the AoA.

As we see in Fig. 8, the accuracy in determining the successive paths is rather good for distances up to 150 m but beyond this distance, it becomes more difficult to extract individual rays. This can be explained by the number of rays arriving during a short time window which become very large when the distance increases, as outlined in Section 3.1. This is the main difficulty when using high resolution algorithms to extract the AoA/AoD in such perfectly guiding structure without obstacles. These algorithms are usually applied to determine the position of the first or last interaction point (reflection or diffraction) between the rays and an obstacle, but with a rather small number of rays. One can also recall that the antennas were placed at a height of 1 m from the ground. At large distances, taking this small height into account, the direct ray cannot be separated from the single-bounce ray corresponding to ground specular reflection. Despite this difficulty, such an approach would

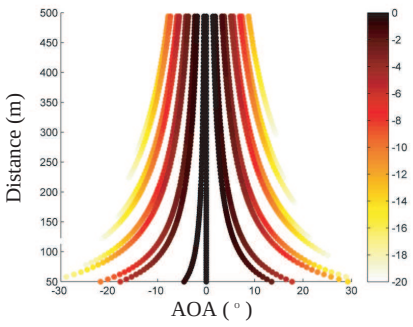

Figure 7. Normalized theoretical $APS(d,\varphi)$, in dB, related to the angle of arrival (AoA) and deduced from the position of the images of the transmitter in a rectangular tunnel. The color scale gives the weight of each ray in dB. The variation of the APS versus distance is quite similar to the variation of the delay spread, grazing rays only playing an important role.

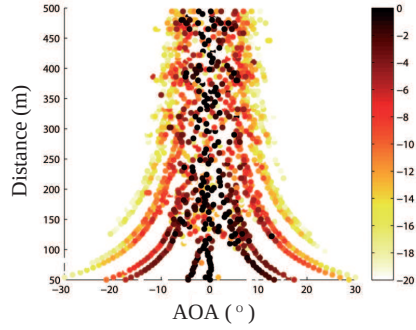

Figure 8. Normalized estimated $APS(d,\varphi)$, in dB, related to the angle of arrival (AoA) and obtained by the high resolution algorithm from the theoretical channel transfer functions. Comparing Figs. 6 and 7 show the difficulty of extracting precise values of the APS when the delay between paths becomes smaller and smaller.

allow getting quantitative experimental values of the angular spread versus the distance between Tx and Rx.

The $APS\ (d,\ \varphi)$ of the AoA deduced from the measured channel transfer functions is given in Fig. 9. We find of course the well known result that the APS decreases with the distance but the spread of the AoA in this arched tunnel is qualitatively smaller than for the theoretical case of a rectangular tunnel (Fig. 8). This agrees with a similar statement made in Section 3.2 about the delay spread.

We also note a slight negative biasing of the AoA which can probably due to an inaccuracy when positioning the fixed virtual array.

To quantitatively establish the variation of the spread of the AoA/AoD versus distance, the angular spread was calculated. This suitable measure of the extent of dispersion in direction related to the AoA is given by (2), provided that the average impinging power $APS\ (d,\ \varphi)$ is highly confined around a certain azimuth. In other cases, ambiguity may appear because of the periodicity of the azimuthal angle [27, 28].

$$\mathrm{AoA}^{\mathrm{rms}}(d) = \sqrt{\frac{\sum\limits_k APS(d,\varphi_k)\,\varphi_k^2}{\sum\limits_k APS(d,\varphi_k)} - \left(\frac{\sum\limits_k APS(d,\varphi_k)\,\varphi_k}{\sum\limits_k APS(d,\varphi_k)}\right)^2}, \quad (2)$$

where φ_k refers to the AoA of path k. A similar formula applies to the AoD.

In Fig. 10, we see that the variations in $\mathrm{AoA}^{\mathrm{rms}}$ and $\mathrm{AoD}^{\mathrm{rms}}$ versus distance are quite similar. The angular spread decreases from 10° at

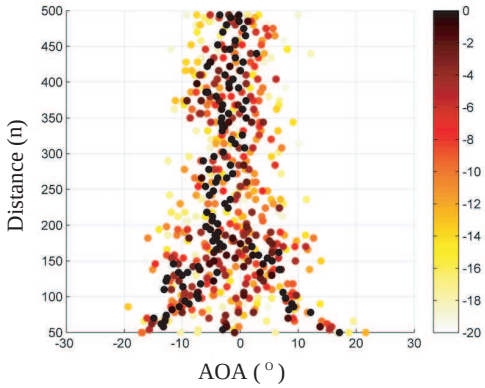

Figure 9. Normalized $APS(d,\ \varphi)$ of the angle of arrival (AoA), expressed in dB, deduced from measurements.

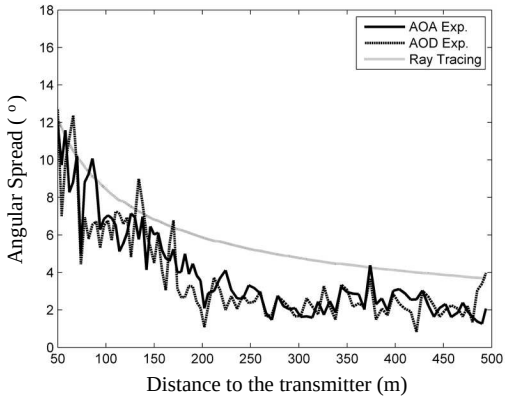

Figure 10. RMS angular spread versus the distance between Tx and Rx, deduced from experiments (AoA Exp. and AoD Exp.) and from a ray tracing approach. The decrease of the angular spread with distance is still a consequence of the importance of rays impinging the walls with a grazing angle of incidence.

50 m from Tx to about 3° at 200 m and then remains nearly constant beyond this distance.

The theoretical angular spread deduced from ray tracing in a rectangular tunnel, and assuming an infinite bandwidth is also plotted in Fig. 10. In this case a continuous decrease is found since there are no constructive/destructive interactions among rays. Due to the symmetry of the problem, theoretical results are the same for AoA and AoD. The angular spread rapidly decreases from 11° to 6° at 200 m, and then to 4° at 500 m.

5. CONCLUSION

Multidimensional propagation characteristics in an empty straight arc-shaped tunnel were deduced from numerous measurements points, the distance between the transmitter and the receiver varying from 50 m up to 500 m. We have shown that the rms delay spread, in the order of 5 ns at 50 m, decreases in the first 100 m but then remains at a fairly constant value of 2.5 ns at larger distances. The guiding feature of the tunnel was also clearly emphasized by the small values of the angular spread of the angle of departure/arrival, rapidly decreasing from 10° at 50 m from the transmitter to 3° at 200 m. The theoretical results deduced from the ray theory assuming a rectangular tunnel slightly overestimate delay spread and angular spread, the curved shape of the

tunnel ceiling being not taken into account, but the variations of these characteristic parameters with distance are quite similar.

ACKNOWLEDGMENT

This work was supported by the Ministerio de Educación y Ciencia, Spain (TEC2010-20841-C04-03), and the Fundación Séneca of Murcia, Spain (08818/PI/08, 14809/EFPI/10 and 06640/FPI/07), by the European FEDER funds, the Region Nord Pas de Calais and the French Ministry of Research, as part of the International Campus on Safety and Intermodality in Transportation Systems (CISIT) project (France).

REFERENCES

1. Zhang, Y. P., G. X. Zheng, and J. H. Sheng, "Radio propagation at 900 MHz in underground coal mines," *IEEE Trans. Antennas Propag.*, Vol. 49, No. 5, 757–762, May 2001.
2. Liénard, M. and P. Degauque, "Natural wave propagation in mine environments," *IEEE Trans. Antennas Propag.*, Vol. 48, No. 9, 1326–1339, Sep. 2000.
3. Boutin, M., A. Benzakour, C. L. Despins, and S. Affes, "Radio wave characterization and modeling in underground mine tunnels," *IEEE Trans. Antennas Propag.*, Vol. 56, No. 2, 540–549, Feb. 2008.
4. Zhi, S. and I. F. Akyildiz, "Channel modeling and analysis for wireless networks in underground mines and road tunnels," *IEEE Trans. on Commun.*, Vol. 58, No. 6, 1758–1768, Jun. 2010.
5. Lienard, M. and P. Degauque, "Propagation in wide tunnels at 2 GHz: A statistical analysis," *IEEE Trans. on Vehicular Techno.*, Vol. 47, No. 4, 1322–1328, Nov. 1998.
6. Zhang, Y. P. and Y. Hwang, "Characterization of UHF radio propagation channels in tunnel environments for microcellular and personal communications," *IEEE Trans. on Vehicular Techno.*, Vol. 47, No. 1, 283–296, Feb. 1998.
7. Molina-Garcia-Pardo, J.-M., M. Lienard, and P. Degauque, "Propagation in tunnels: Experimental investigations and channel modeling in a wide frequency band for MIMO applications," *EURASIP J. on Wireless Communications and Networking*, Article ID 560571, 9 pages, 2009, doi:10.1155/2009/560571.
8. Valdesuerio, J. A., B. Izquierdo, and J. Romeu, "On 2×2 MIMO observable capacity in subway tunnels at X-Band: An

experimental approach," *IEEE Antennas and Propag. Letters*, Vol. 9, 1099–1102, 2010.

9. Molina-Garcia-Pardo, J. M., M. Lienard, P. Degauque, E. Simon, and L. Juan Llacer, "On MIMO channel capacity in tunnels," *IEEE Trans. on Antennas and Propag.*, Vol. 57, 1–10, Dec. 2009.
10. Didascalou, D., T. M. Schäfer, F. Weinmann, and W. Wiesbeck, "Ray density normalization for ray-optical wave propagation modeling in arbitrarily shaped tunnels," *IEEE Trans. Antennas Propag.*, Vol. 48, No. 9, 1316–1325, Sep. 2000.
11. Popov, A. V. and N. Y. Zhu, "Modeling radio wave propagation in tunnels with a vectorial parabolic equation," *IEEE Trans. Antennas Propag.*, Vol. 48, No. 9, 1403–1412, Sep. 2000.
12. Wang, T.-S. and C.-F. Yang, "Simulations and measurements of wave propagations in curved road tunnels for signals from GSM base stations," *IEEE Trans. Antennas Propag.*, Vol. 54, No. 9, 2577–2584, Sep. 2006.
13. Araujo, M. G., F. Obelleiro, and J. L. Rodriguez, "Modeling high frequency propagation in tunnel environments by iterative physical optics methods," *Wireless Pers. Comm.*, Vol. 20, No. 3, 237–250, Mar. 2002.
14. Ndoh, M., G. Y. Delisle, and R. Le, "A novel approach to propagation prediction in confined and diffracting rough surfaces," *Int. J. Num. Modeling: Electron. Networks, Devices and Fields*, Vol. 16, No. 6, 535–555, Dec. 2003.
15. Mahmoud, S. F., "Wireless transmission in tunnels with non-circular cross section," *IEEE Trans. Antennas and Propag.*, Vol. 58, No. 2, 613–616, 2010.
16. Hadi, M. F. and S. F. Mahmoud, "Modelling wireless propagation in a rectangular tunnel with the compact-FDTD method," *IEEE Radio and Wireless Symp.*, Jan. 22–24, 2008.
17. Emslie, A. G., R. L. Lagace, and P. F. Strong, "Theory of the propagation of UHF radio waves in coal mine tunnels," *IEEE Trans. Antennas Propag.*, Vol. 23, 192–205, 1975.
18. Mahmoud, S. F. and J. R.Wait, "Geometrical optical approach for electromagnetic wave propagation in rectangular mine tunnels," *Radio Sci.*, Vol. 9, 1147–1158, 1974.
19. Holloway, C. L., D. A. Hill, R. A. Dalke, and G. A. Hufford, "Radio wave propagation characteristics in lossy circular waveguides such as tunnels, mine shafts and boreholes," *IEEE Trans. Antennas Propag.*, Vol. 48, 1354–1366, Sept. 2000.

20. Dudley, D. G. and S. F. Mahmoud, "Linear source in a circular tunnel," *IEEE Trans. Antennas Propag.*, Vol. 54, No. 7, 2034–2047, Jul. 2006.
21. Mahmoud, S. F., "Modal propagation of high frequency EM waves in straight and curved tunnels within the earth," *Journal of Electromagnetic Waves and Applications*, Vol. 19, No. 12, 1611–1627, 2005.
22. Molina-Garcia-Pardo, J. M., M. Lienard, A. Nasr, and P. Degauque, "On the possibility of interpreting field variations and polarization in arched tunnels using a model for propagation in rectangular or circular tunnels," *IEEE Trans. Antennas Propag.*, Vol. 56, No. 4, 1206–1211, Apr. 2008.
23. Didascalou, D., J. Maurer, and W. Wiesbeck, "Subway tunnel guided electromagnetic wave propagation at mobile communications frequencies," *IEEE Trans. Antennas Propag.*, Vol. 49, No. 11, 1590–1596, 2001.
24. Rappaport, T. S., *Wireless Communications, Principles and Practice*, Prentice Hall Ed., 1999.
25. Richter, A. and R. Thoma, "Joint maximum likelihood estimation of specular paths and distributed diffuse scattering," *Proc. of the IEEE Int. Conf. on Vehicular Techno.*, Vol. 1, 11–15, May 30–Jun. 1, 2005.
26. Richter, A., "Estimation of radio channel parameters: Models and algorithms," Ph.D. Dissertation, Technische Univ. Ilmenau, Ilmenau, Germany, 2005.
27. Molisch, A. F., *Wireless Communications*, IEEE Press and Wiley Ltd., 2005.
28. Eggers, P., "Angular propagation descriptions relevant for base station adaptive antenna operations," *Kluwer Wireless Personal Commun.*, Vol. 11, 3–29, 1999.